9

Micro-Welding of Super Thermal Conductive Composite by Pulsed Nd:YAG Laser

Mohd Idris Shah Ismail[1,2], Yasuhiro Okamoto[1] and Akira Okada[1]
[1]*Graduate School of Natural Science and Technology, Okayama University*
[2]*Department of Mechanical & Manufacturing Engineering, Universiti Putra Malaysia*
[1]*Japan*
[2]*Malaysia*

1. Introduction

The diffusion of generated heat in the electronic devices is an important issue. The heat would be diffused from electronic devices by passive strategies, which would be carried out by the use of high thermal conductivity materials as a heat sink. The development of advanced materials with the superior high-thermal properties and the high strength-to-weight ratio has led to new metal matrix composites (MMCs) as a great attractive material in the electrical and electronic industries. Aluminum and its alloys are widely used for the manufacturing of MMCs, which have reached the industrial stage in some areas (Barekar et al., 2009). In order to manufacture practical components from MMCs, a technique for joining MMCs to other similar composites or to monolithic materials is strongly required. Therefore, the development of reliable and economic joining technique is important for extending the applications of MMCs. It is well-known that laser welding is the most flexible and versatile welding technology, and it has succeeded in the welding of MMCs (Niu et al., 2006; Bassani et al., 2007).

Recently, a super thermal conductive (STC) aluminum-graphite (Al-Gr) composite with the high thermal conductivity and the low coefficient of thermal expansion (CTE) was developed (Ueno et al., 2009). The properties of thermal conductivity versus thermal expansion coefficient are summarized in Figure 1, where the upper ellipse zone shows the STC composite materials, and the other of conventional thermal conductive materials such as Cu, Al, Al-SiC, Cu-W, Cu-Mo, AlN and Si are also indicated. It is difficult to weld STC Al-Gr composite material compared with existing MMCs, since the graphite material only can be melted under the high pressure with the high temperature (Kirillin & Kostanovskii, 2003). In the laser welding, the use of standard pulse profile is limited to joint this material, since the uncontrolled heat input generates an overshoot, which leads to undesirable welded joints. The control of heat input by a pulse waveform is very important to achieve a suitable welding penetration, preventions of overheating and unacceptable welding defects.

In this study, the welding of STC Al-Gr composite was experimentally and numerically investigated by using a pulsed Nd:YAG laser with the control of pulse waveforms, which

can provide a well-controlled heat input with high energy density. These investigations have led to an optimum welding condition proposed for a pulsed laser welding with minimum weld defects. The experimental work was carried out in two sections, namely the bead-on-plate welding of STC Al-Gr composite, and the overlap welding of pure aluminum and STC Al-Gr composite. The welding characteristics of STC Al-Gr composite were discussed by the observation of joint part with optical microscope, scanning electron microscope (SEM) and energy dispersive spectroscopy (EDS). Moreover, the temperature distributions in the laser micro-welding process were numerically analyzed to discuss the proper heat input. The weld strength was also evaluated by a shearing test for the overlap welding with and without the control of pulse waveform.

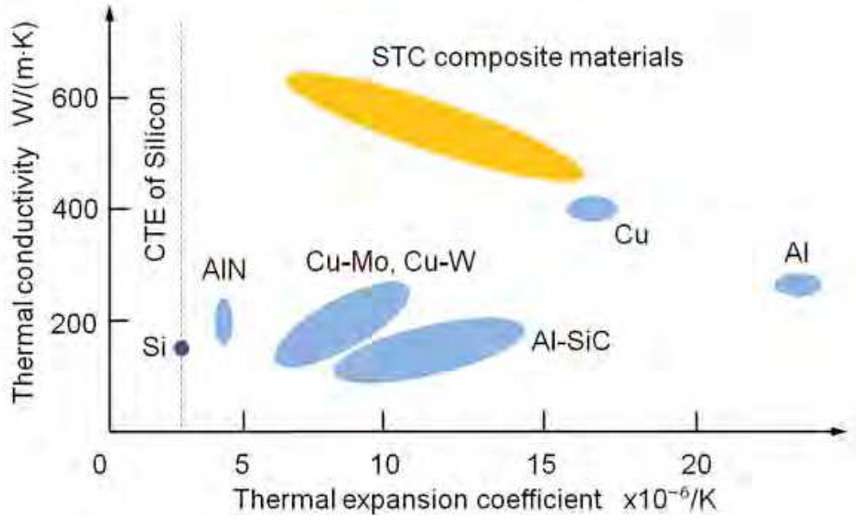

Fig. 1. Thermal conductivity and thermal expansion coefficient of STC composites and other materials

2. Background and overview

Each material has its own unique properties. In many applications, it has been found that there is a need for the combination of several properties together. These desired material property combinations can be achieved by the development of new composite materials. Composite materials are usually classified by the type of material used for the matrix. The four primary categories of composites are polymer matrix composites (PMCs), metal matrix composites (MMCs), ceramic matrix composites (CMCs), and carbon-carbon composites (CCCs) (Kutz, 2002). In this study, the viewpoint was MMCs, which having the properties of lightweight, high specific strength, wear resistance, and a low coefficient of thermal expansion.

Aluminum has many properties such as high thermal and electrical conductivity, high corrosion resistance, low cost and lightweight that make it ideal for use in MMCs. In addition, aluminum can be recycled and offers intriguing environmental and economical opportunities (Cannillo et al., 2010). From the chemical point of view, the aluminum reacts with carbon to form only aluminum carbide (Al_4C_3) intermetallic compounds as shown in the Figure 2. The Al_4C_3 is known as the only stable intermediate in the Al-C binary system. However, it is very brittle at the ambient temperature (Lu et al., 2001). Based on the Al-C

phase diagram (Massalski et al., 1990), it can be seen that the coexistence of liquid aluminum and solid carbon requires the existence of an intermediate phase Al_4C_3. At equilibrium phase, it is impossible to directly dissolve solid carbon into liquid aluminum unless the temperature is above the melting point of Al_4C_3 (Lu et al., 2001). Graphite, in the form of fibers or particulates has been recognized as a high-strength and low density material (Barekar et al., 2009). The material combination of aluminum and graphite could produce an advanced aluminum-graphite (Al-Gr) composite, which has an unique thermal properties, due to to the opposite thermal expansion coefficients of aluminum and graphite.

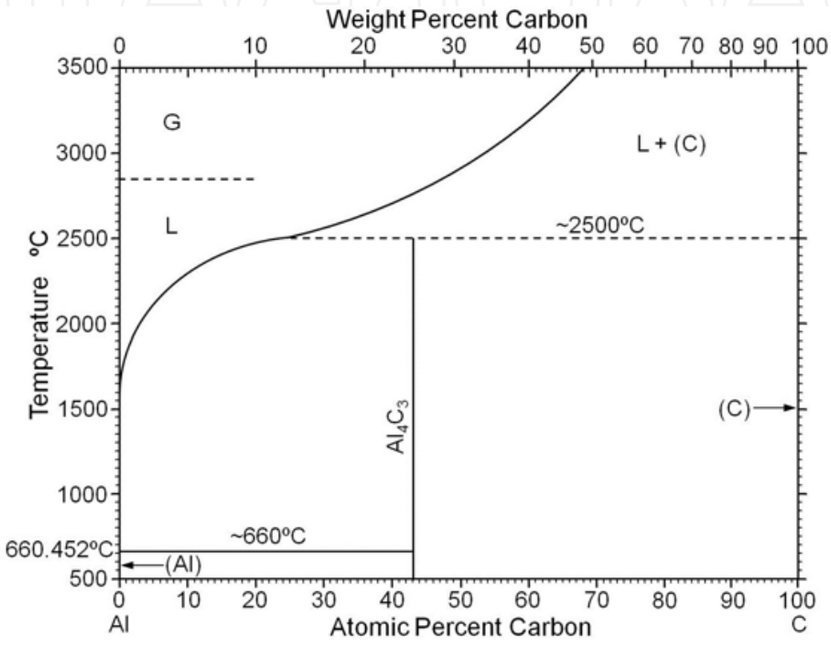

Fig. 2. Al-C phase diagram

Recently, a super thermal conductive(STC) Al-Gr composite was developed, which have been prepared by utilizing a pulsed electric current sintering method (Ueno et al., 2009) to realize the properties of higher thermal conductivity and lower thermal expansion coefficient. The material properties of STC Al-Gr composite are shown in Table 1. It shows that the thermal conductivity, thermal expansion coefficient and bending strength are anisotropic due to the directional properties of graphite and their designed orientation in xy plane-direction (top view) and xz thickness-direction (section view) as shown in Figure 3.

The demand for lighter and thinner products has led MMCs to be manufactured, especially in welding process. The welding process of MMCs has attracted various industries by the reduction of material weight and costs, and improvement of design flexibility. Therefore, the development of efficient, flexible and reliable joining technique is significantly important to increase the potential of MMCs. Compared with the conventional fusion welding techniques, laser welding has numerous advantages such as narrow heat-affected zone (HAZ), good quality of weld bead, precise positioning and control of irradiation beam and its movement, the ease of automation and the high production speed (Behler et al., 1997; Pan et al., 2004). Laser welding is characterized by intermittent laser beam powers that would

allow melting and solidification consecutively. The great advantage of laser welding is keyhole effect by very high power densities involved in the laser welding, which makes laser welding technique widely used in many industrial productions.

Material properties		Value
Thermal conductivity	k_{xx} , k_{yy}	450 W/(m·K)
	k_{zz}	40 W/(m·K)
Specific heat	c	810 J/(kg·K)
Density	ρ	2450 kg/m³
Thermal expansion coefficient	α_{xx} , α_{yy}	17×10^{-6}/K
	α_{zz}	8×10^{-6}/K
Bending strength	M_{xx}	65 MPa
	M_{zz}	7 MPa
Tensile strength	σ	49 MPa
Young modulus	G	31 GPa
Electrical resistivity	R	17×10^{-8} Ωm

Table 1. Material properties of STC Al-Gr composite

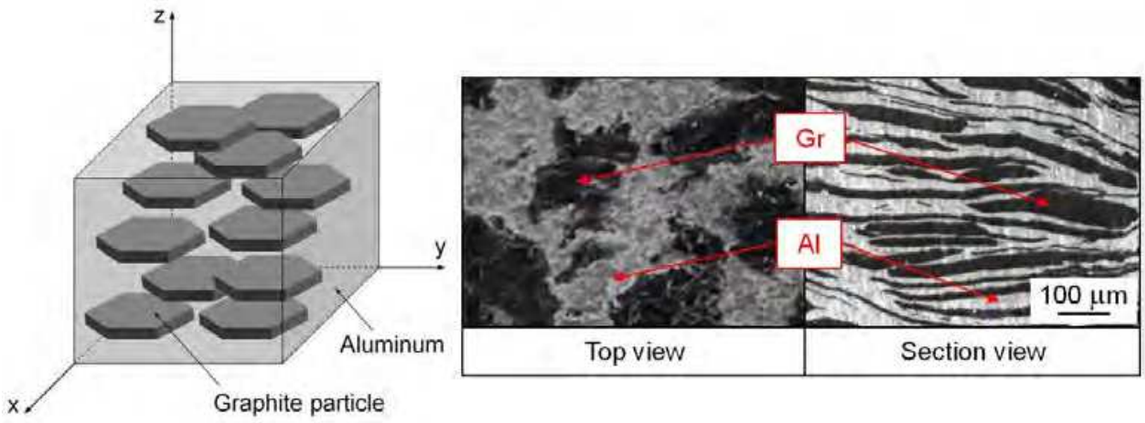

Fig. 3. Schematic illustration and optical micrographs of STC Al-Gr composite

Since the STC Al-Gr composite is a new composite in MMCs, no work has been reported concerning the welding behaviour on this composite by laser welding technique. There are several published papers related to the laser welding of MMCs, especially in the composites with combination of Al and SiC. Niu et al. (2006) reported that the welding of Al-SiC can be successfully realized by using laser welding. It is possible to control the geometry of weld bead by precisely controlling the laser output parameters (Yue et al., 1996). However, the reaction between SiC and Al in the weld zone generates a formation of needle-like brittle Al_4C_3, which can degrade the mechanical properties of Al-SiC composite. It dissolves in aqueous environments resulting in a loss of integrity to the weld zone (Lienert et al., 1993).

In addition, the Al_4C_3 formation reduces the toughness of the weld bead, even it results in the increase of hardness (Bassani et al., 2007). Therefore, preventing the formation of the Al_4C_3 during welding process is important for successful welding of Al-SiC composites (Wang et al., 2000).

There are severe heterogeneity of the material structure and the great difference in both physical and chemical properties between the aluminum matrix and graphite particles. This point would make the welding of STC Al-Gr composites to a challenging technological problem for applying the laser welding technique in the industrial application. In this study, the pulsed Nd:YAG laser was used as a laser source. Square shape pulses are the standard output of this laser with the constant power distribution during its duration time. By utilizing the ability of pulsed Nd:YAG laser to shape the temporal power profile of each pulse offers the high flexibility in optimising the weld parameters. This pulse waveform allows the control of penetration, melt pool geometry and keyhole formation. It also has been reported that pulse waveform to be an effective method to reduce or eliminate the weld defects (Zhang et al., 2008).

3. Experimental procedures

A schematic diagram of experimental setup is shown in Figure 4. In this study, a pulsed Nd:YAG laser (LASAG SLS200 CL8) of 1064 nm in wavelength was used as a laser source. The laser beam was collimated to 15 mm in diameter and delivered by an optical fiber of 50 μm core diameter. The collimator was installed between the optical fiber and the bending mirror, and the collimated laser beam was focused on the specimen surface by a lens of 50 mm in focal length. In order to avoid the back-reflection of incident laser beam, the processing head was aligned by 10 degrees to the perpendicular axis of the specimen surface. The irradiation experiments were carried out in two sections, namely the bead-on-plate welding of STC Al-Gr composite, and the overlap welding of pure aluminum and STC Al-Gr composite. The welding experiments were done in a shielding gas of nitrogen with 13L/min flow rate. The stage controller could determine the movement of X-Y-Z stage, and it also synchronized the laser pulse.

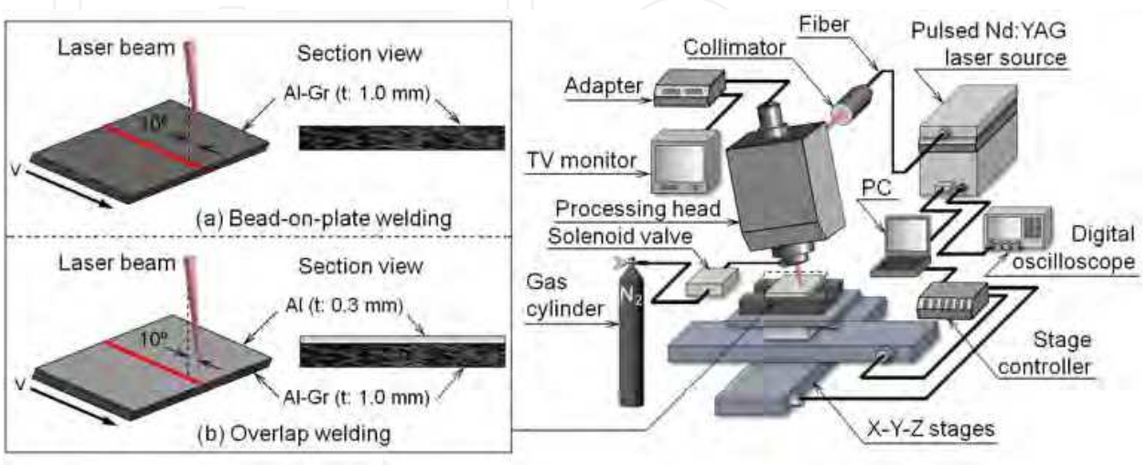

Fig. 4. Schematic diagram of experimental setup

After the laser welding, the sectioned surface of welded specimen was ground, polished and etched for the observation of weld bead by an optical microscope, scanning electron microscope (SEM) and energy dispersive spectroscopy (EDS). In addition, the shearing test was carried out to measure the shear strength of the overlap welded joints with a Shimadzu EZ-L test machine. The specimen for shear strength of overlap welding was designed with five seam lines and 1.5 mm distance between each line as shown in Figure 5. The cross-head speed was set to 0.5 mm/min. The specimen was gripped by the clampers, which are placed in the fixture blocks. Then, a shear load was slowly increased at the suitable increments by the mechanical lever system until the welded joint of specimen was fractured. The shear strength was calculated by using fracture load and welding area. The value of shear strength was the average of three specimens. Then, the fracture surfaces were examined with SEM and EDS analysis.

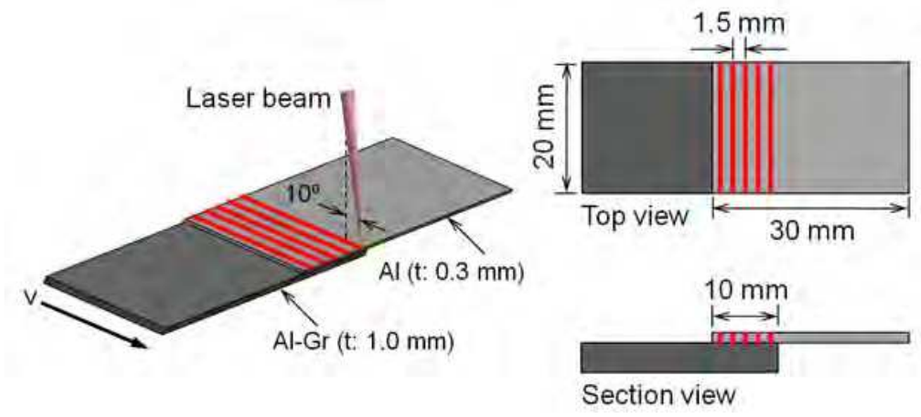

Fig. 5. Configuration of shearing test specimen

4. Thermal analysis by finite element method

In this study, the further analysis of the welding phenomenon was discussed by the heat conduction analysis with finite element method (FEM) to simulate the thermal process of laser welding. The analysis model is based on the fundamental heat transfer for the laser welding process. Based on the first law of thermodynamics, the heat flow in a three-dimensional solid can be expressed as equation (1) (Kannatey-Asibu, 2009)

$$\rho \cdot c(\theta)\frac{\delta\theta}{\delta t} = \frac{\delta}{\delta x}\left[k(\theta)\frac{\delta\theta}{\delta x}\right] + \frac{\delta}{\delta y}\left[k(\theta)\frac{\delta\theta}{\delta y}\right] + \frac{\delta}{\delta z}\left[k(\theta)\frac{\delta\theta}{\delta z}\right] + Q_v \quad (1)$$

where ρ, $c(\theta)$, $k(\theta)$ and Q_v are the material density, the temperature dependent specific heat, the temperature dependent thermal conductivity and the volumetric heat source term which varies with a laser power. $\theta=\theta(x,y,z,t)$ is the resulting three-dimensional and temporal temperature distribution in the material. t is time, and x, y, z are the spatial Cartesian coordinates.

Figure 6 shows the developed finite element models for bead-on-plate welding and overlap welding. Fine mesh resolution is given at and near the heat source, while a fairly coarse mesh density is considered at the region far from the heat source. A portion of the

specimens was designed in the analysis model in order to reduce the calculation time. In addition, the half model with symmetric conditions is used in the analysis. As the heat source of laser beam is symmetric in the x-z plane, only half the heat source is considered. The heat source comprises a Gaussian plane heat source on the top surface and a conical shape heat source along the thickness of the specimen. To simplify the analysis, it was assumed that the alignment of laser spot was perpendicular to the specimen surface and a single spot of laser irradiation was utilized in the heat conduction analysis. The convective heat transfer condition of air was considered after the set time of laser irradiation. Except for a laser beam irradiated area, the convective heat transfer condition of air was also assumed. The main FEM analytical conditions are shown in Table 2.

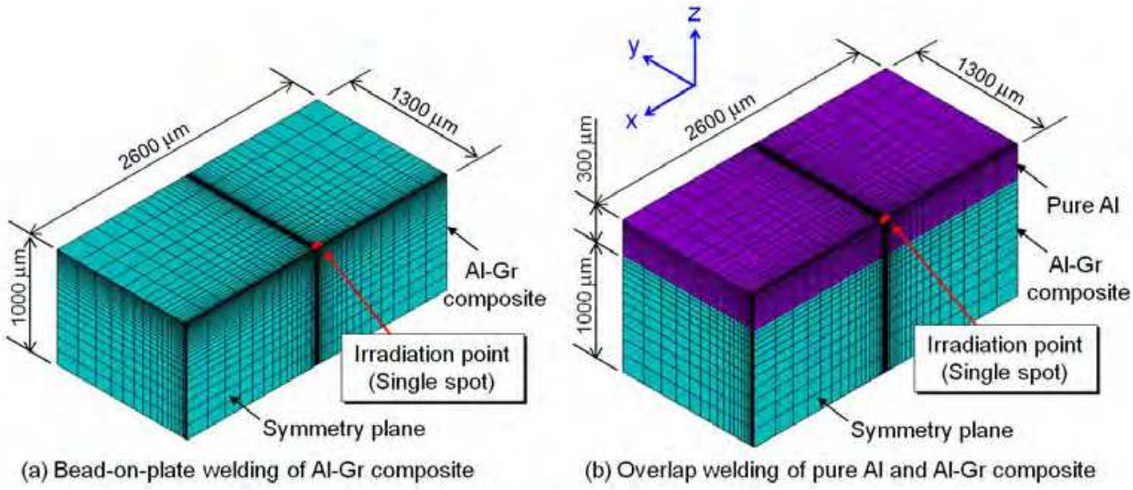

Fig. 6. Finite element models for investigation of temperature distributions

Parameter/condition		Bead-on-plate welding	Overlap welding
Laser power	P	20, 30, 40 W	400 W
Pulse width	τ	1.5 ms	2.7, 3.0, 5.0 ms
Beam diameter	d	50 µm	
Heat transfer coefficient	h	10 W/(m²·K)	
Room temperature	θ_{room}	293 K	

Table 2. FEM analysis conditions

5. Bead-on-plate welding

In the bead-on-plate welding experiment, the STC Al-Gr composite of 1 mm thickness was used as the specimen. The specimen was mounted by clamping fixture with the alumina-ceramic plates, which are located on the bottom surface of specimen to minimize the heat loss during welding experiments. The rectangular shape of laser pulse was fixed as the standard output of laser source. The experiments were conducted with laser power up to 50 W, pulse width from 1 to 5 ms and scanning velocities varied between 12 to 72 mm/min.

5.1 Influence of welding parameters

In the first experiment, the welding condition on the top surface of Al-Gr composite was investigated by changing the power of laser pulse. The pulse width, pulse repetition rate and scanning velocity were kept constant at 1 ms, 5 Hz and 12 mm/min, respectively. The results of this experiment are shown in Figure 7. It can be noticed that the laser power significantly affected the welding condition. As shown in figure, when the laser power is insufficient high, the molten zone was discontinuous. At the lower 20 W of laser power, the molten zone can be observed only on the aluminum material, while the graphite material is non-molten phase. It is consider that the insufficient laser energy would not react the graphite material.

It is assumed that too high laser power leads to the generation of weld defects with increasing the power density. In practice, the power density below 10^7 W/cm^2 is generally advisable to avoid severe ejection of molten material (Cao et al., 2003). At the 50 W of laser power it seems too high power density resulting blowholes and a poor quality of weld surface. The power density on the specimen surface can be reduced to prevent the porosities at the weld pool surface by reducing the laser power. Therefore, the acceptable condition of weld surface is obtained between 30 W to 40 W of laser power. However, since the graphite element only can be melted under the high pressure with high temperature (Kirillin & Kostanovskii, 2003), the existence of this element in the molten zone of Al-Gr composite is important to identify. It might be considered that the required laser power to generate molten zone in this composite is relatively smaller than the welding of pure aluminum, even it has a higher thermal conductivity.

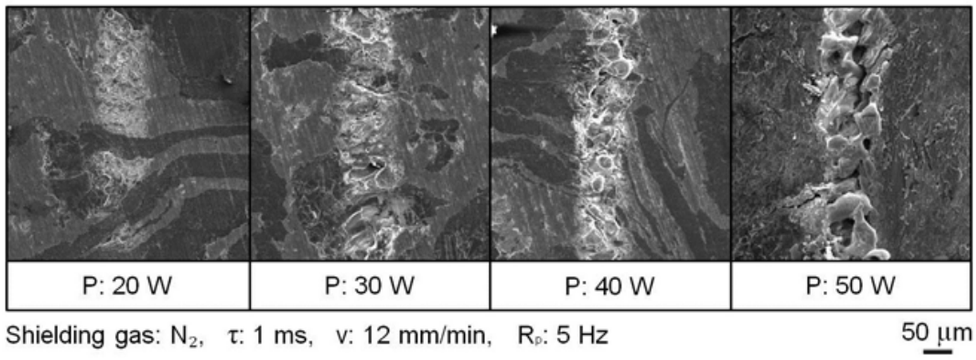

Fig. 7. Influence of laser power on the top surface of weld bead

In order to identify the presence of graphite element in the molten zone, the energy-dispersive X-ray spectroscopy (EDS) technique was used for the elemental analysis. Figure 8 shows the distribution map of elements Al and C on the top surface of molten zone. As shown in the figure, the element Al is the main composition detected in the molten zone. However, the EDS mapping shows that only small particles of graphite were observed on the top of the solidified aluminum. Judging from the distribution maps of elements, it can be presumed that the graphite was not mixture with aluminum, and it was ruptured into small particles. Even the aluminum material of Al-Gr composite was melted with the low laser power, the graphite material could not be melted. Because, the graphite only can be melted at the high temperature (θ_{melt}: 4765 K) under the high pressure (F_{melt}: 100 bar) (Joseph et al.,

2002) compared with the melting point of aluminum (θ_{melt}: 933 K). In addition, since the graphite is soft and brittle material, the graphite would be smashed only by direct irradiated laser beam to form the small particles during keyhole welding process.

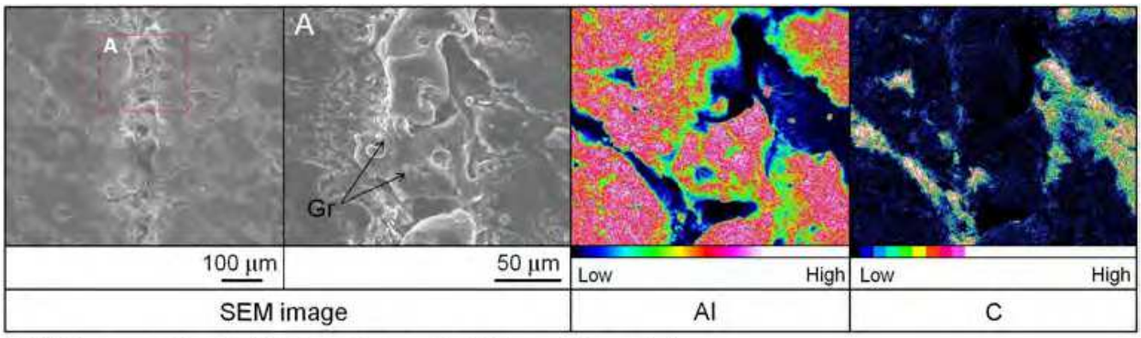

Fig. 8. SEM photographs and element mapping of Al and C

In the second series of welding experiments, the influence of pulse width was investigated. Figure 9 shows the appearance of weld beads under the various pulse widths at a constant laser power. It shows that the longer pulse width would generate more molten volume because the weld pool remains for an extended period of time. The widest welds are generated by the longer pulse width, which is considered due to the longer heating time. As a result, the irregular shapes and large size of cavities or blowholes are generated periodically when the pulse width was more than 1 ms. The tendency of blowhole occurrence and weld bead imperfections were drastically increased in the case of longer pulse width due to instabilities of the keyhole. In addition, the adverse effect of long pulse width on the weld penetration was believed due to a higher proportion of heat conducted laterally into the specimen. The results reflect that the higher energy input would enlarge processed zone. As mentioned later in section 5.2, based on the thermal analysis by FEM, a very short pulse width is enough to initiate the melting of aluminum and the evaporation of graphite on the welding of Al-Gr composite.

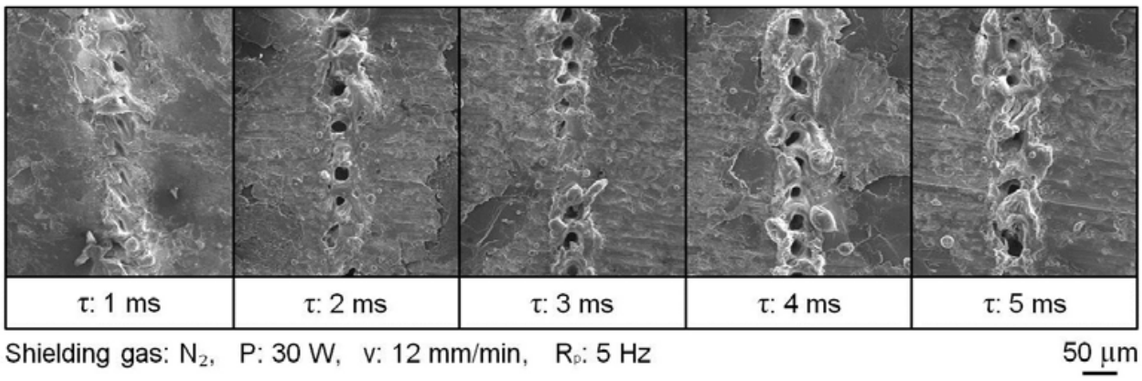

Fig. 9. Influence of pulse width on the top surface of weld bead

In order to keep the continuity of the penetration, the overlapping ratio was kept constant at 20 %. An increase in scanning velocity would increase the pulse repetition rate in the pulsed

laser welding. The influence of scanning velocity on the top surface of weld bead was shown in Figure 10. It is noted that with the decrease of scanning velocity led to the enhancement of the molten zone surface, in which the weld seam surface showed an uniform surface ripple formation without blowholes. It can be seen that the effect of the remaining energy of the previous pulse is significant to interact the Al-Gr composite by the subsequent laser pulse. However, the size of molten zone was wider at the higher scanning velocity with the blowholes and poor quality of weld surface. Because the scanning velocity matches an opposite with the heat input, and the increasing of the scanning velocity means the decreasing of the average power per unit weld length exerted on the welding line, thereby producing a small amount of intermixed melt. Therefore, the lower scanning velocity is required to produce acceptable welded joints and maintain welding quality.

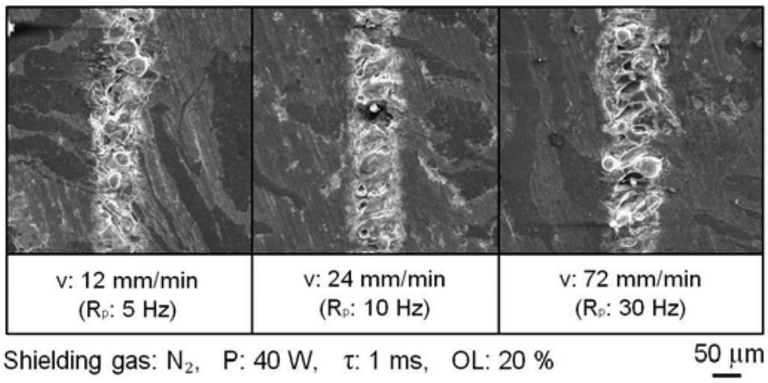

Fig. 10. Influence of scanning velocity on the top surface of weld bead

5.2 Temperature field induced in STC Al-Gr composite

A thermal analysis was carried out, in order to study the temperature field induced in the welding process of Al-Gr composite**.** Figure 11 and 12 show the influence of laser power and pulse width on temperature distribution of Al-Gr composite spatially and temporally. It can be clearly clarified that the absorbed energy on the Al-Gr composite was quickly removed in x-direction compared to the *z*-direction due to the higher thermal conductivity in x-direction (k_{xx}: 450 W/(m·K)), which is more than ten times of the thermal conductivity in z-direction (k_{zz}: 40 W/(m·K)). It can be seen that the increase of laser power and pulse width could enable an elevated temperature. This can be described that an enhanced laser energy input is absorbed by Al-Gr composite. In particular, when the low laser power of 20 W and 30 W are applied, the maximum temperatures are approximately 2400 K and 3500 K, respectively, which reaches to the melting and evaporation temperature of aluminum material below evaporation temeparture of graphite material. At the higher laser power of 40 W, the evaporation of graphite material occurs because the peak temperature of 4607 K exceeds the evaporation temperature of graphite. However, the influence of pulse width shows the slight increasing on the temperature after the melting of aluminum or evaporation of graphite was achieved. According to the thermal analysis results, it can be concluded that the laser power is significantly influenced on the evaporation of graphite. Judging from these results, a very short pulse width is required to initiate the melting of aluminum and the evaporation of graphite on the welding of Al-Gr composite.

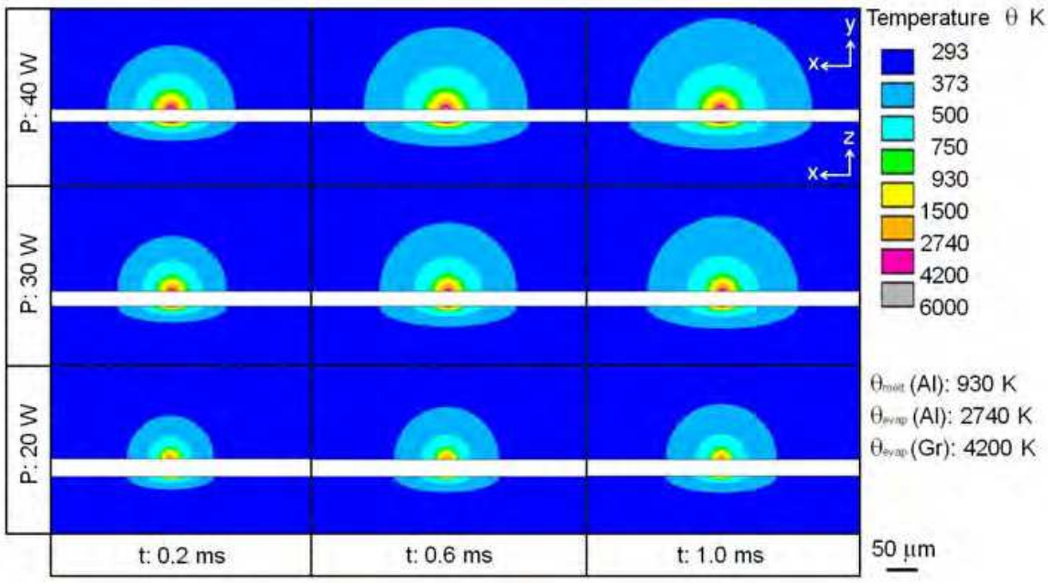

Fig. 11. Spatial temperature distributions in bead-on-plate welding

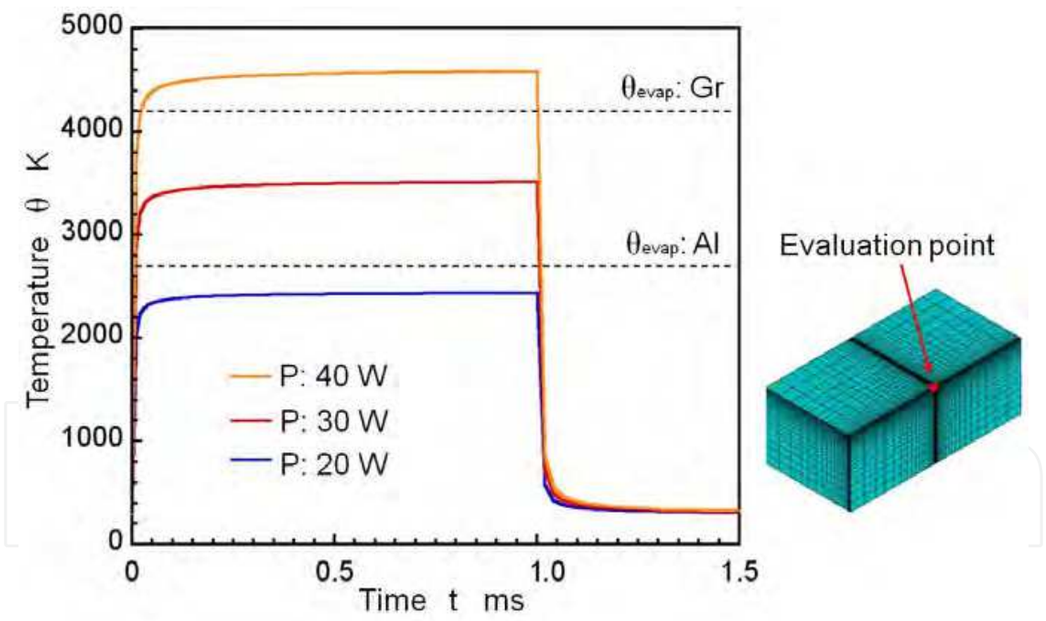

Fig. 12. Temperature histories in bead-on-plate welding

6. Overlap welding

In the overlap welding experiment, the pure aluminum sheet of 0.3 mm thickness and the STC Al-Gr composite of 1 mm thickness were used as the specimens. In order to achieve an optimum welding condition, the rectangular and controlled pulse waveforms of laser pulses were utilized as the output of laser source.

6.1 Rectangular pulse waveform

The variations of laser power from 300 to 550 W with constant 1 ms pulse width were irradiated on the specimen of 0.3 mm thickness aluminum and 1.0 mm Al-Gr composite plate as shown in Figure 13. It could be seen that the laser pulse energy less than 400 mJ/pulse was insufficient to form a molten geometry for joining both materials, in which the penetration depth was shallow. The higher pulse energy was crucial to achieve the sufficient penetration depth and control the formation of molten geometry. However, the cross-section view above 450 mJ/pulse showed signs of porosity and bump defects. Moreover, the undercut defect was observed at the higher pulse energy of 550 mJ/pulse. Judging from these observation results, it was confirmed that the higher laser power (more than 400 W) causes destructive effects, and lower laser power (less than 400 W) will restrict the penetration depth and joining. From these viewpoints mentioned above, the next welding experiments were carried out under the constant 400 W laser power with various pulse widths in the rectangular pulse waveform.

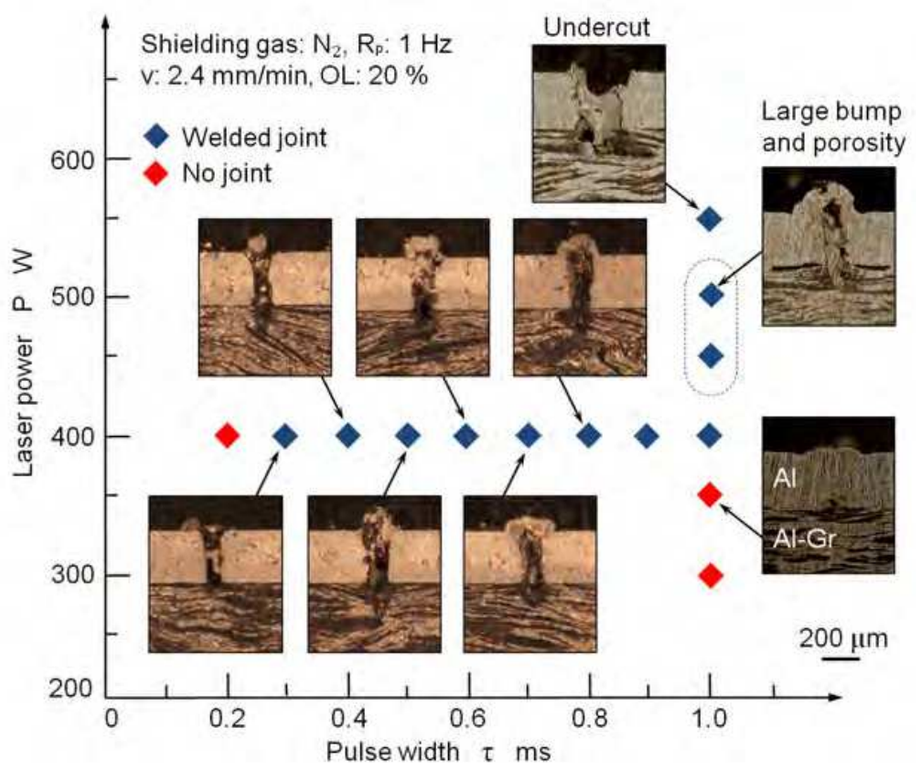

Fig. 13. Welding results with rectangular pulse waveform

Figure 13 shows welding results with the rectangular pulse waveform for various pulse widths and laser powers. As shown in the figure, the width of laser pulses had a significant role on the penetration depth. The weld joint between aluminum plate and Al-Gr composite can be seen at the pulse widths more than 0.3 ms. The penetration depth and bead width gradually increased with increasing the pulse width. However, these increments led to the increase of bump size in the weld joint. On the other hand, the penetration depth increased gradually with increasing the laser pulse energy, and a

joining part between pure aluminum plate and Al-Gr composite was obtained with porosity and bump defects. According to the observation results of cross-section in the welding with rectangular pulse waveform, the pulse width of 0.6 ms was better condition with the deeper penetration, smaller porosities and bumps.

6.2 Controlling pulse waveform

As mentioned in the above observation results of normal rectangular pulse waveform, the bump and porosity defects were the major problem in the overlap welding between pure aluminum and Al-Gr composite. In order to overcome these problems, a controlled pulse waveform is discussed, since it is considered that an appropriate controlled laser pulse waveform could generate a better welded joint. Figure 14 shows the controlled pulse waveform named as a spike pulse waveform. The spike pulse waveform is divided into two phases. At the phase one, the laser power of 400 W and pulse width of 0.6 ms were selected according to the previous experimental results of rectangular pulse waveform. Phase two is a subsequent function of the phase one by adding the heat to melt the bump generated in the phase one. This re-melting process is intended to remove the porosity in order to obtain a better joining state. Therefore, the experiments were carried out to discuss an appropriate value of laser power P_2 and time period t_2 at the phase two of spike pulse waveform.

From the cross-section observation as shows in Figure 15, it was seen that the porosity and bump have remained at a range of laser power 50-125 W, while an undercut was generated at the laser power more than 200W. The observation results of laser power 150 W and 175 W showed acceptable joining conditions, and 175 W was selected as the laser power of phase two (P_2) for the deeper penetration and less porosity defect. The next experiment was carried out to define an optimum pulse width to set the time period t_2 at the phase two of spike pulse waveform as shown in Figure 14.

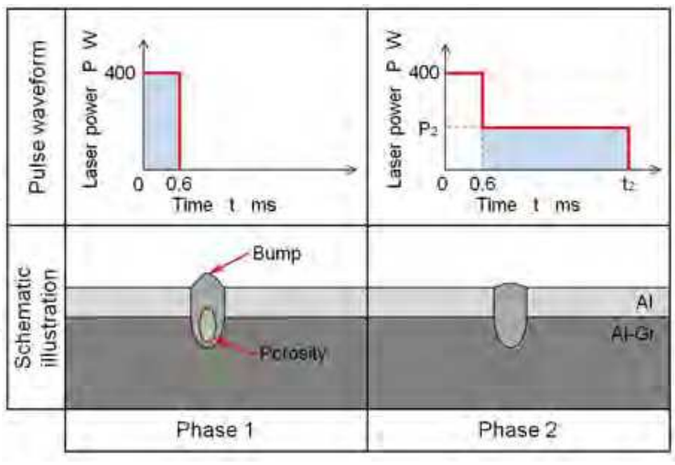

Fig. 14. Schematic illustration of welding process with spike pulse waveform

The pulse width was set less than 5 ms due to the limitation of maximum pulse width in the laser system used in this study. Figure 16 shows the cross-section views for various pulse widths under the same laser power of phase two to define the appropriate value of pulse width at the phase two for the spike pulse waveform. An appropriate irradiation time is necessary to melt and reduce a bump during a welding process. Within the range 1.5-2.5 ms

of pulse width (t_2), the results show that the welding defect of bump was not removed. Moreover, it could be cleared that the longer irradiation time (t_2: 3.5-5.0 ms) generated the larger size of bump. On the other hand, the pulse width t_2 of 3 ms showed an acceptable penetration depth. Judging from these results, 3 ms is selected as an appropriate value of t_2 at the phase two in the case of spike pulse waveform due to the stable penetration and smaller bump without porosities.

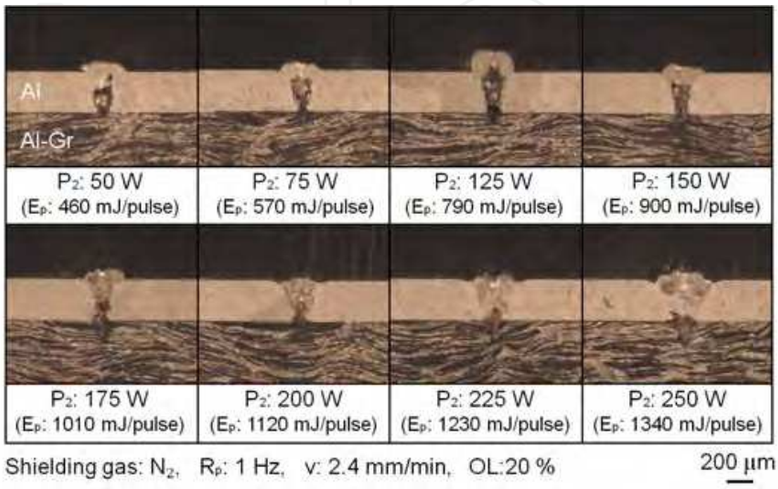

Fig. 15. Influence of laser power (P_2) in phase 2 of spike pulse waveform

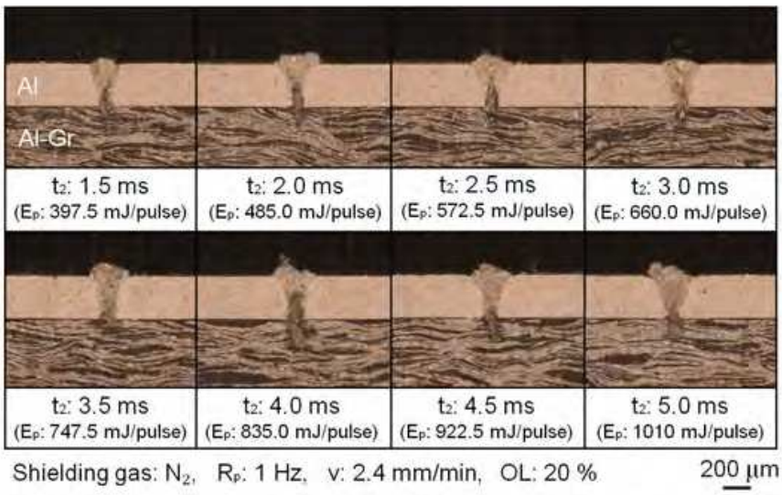

Fig. 16. Influence of pulse width (t_2) in phase 2 of spike pulse waveform

In addition, the elemental analysis was performed to observe the element distribution at the welded parts using a SEM equipped with the energy dispersive spectroscopy (EDS). Figure 17 showed the results of EDS mapping analysis in the case of spike pulse waveform. The shape of molten zone at the Al-Gr composite can not be seen clearly because of too much carbon particles on the molten zone, which can not be melted during the welding process. It could be seen that the coarse carbon located at the welded joint between pure aluminum

and Al-Gr composite. It is considered that the severe convection of graphite particles with aluminum materials might be occurred in the molten zone. In other words, when Al-Gr composite is evaporated, an over-pressure is developed in the keyhole. This phenomenon would cause graphite particles pushed up from the prior zone in Al-Gr composite to the zone in the pure aluminum with melting phase, and finally the carbon particles would be redistributed during the re-solidification. However, it could be seen that a lack of fusion defect was generated by the spike pulse waveform. It could be detected by using an accurate microscopic observation in the high magnification condition. The lack of fusion defect in the molten zone can be identified by its string-like appearance, and it had randomly oriented curvature. It is considered that the lack of fusion defect is not pore, since the carbon element could be seen in this area.

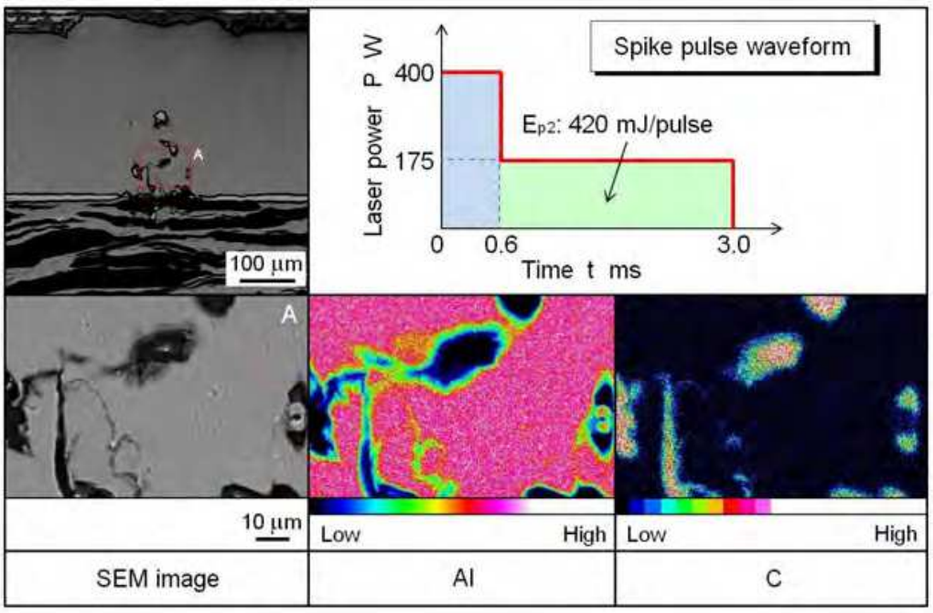

Fig. 17. SEM images and EDS mappings with spike pulse waveform

From the observation results by the spike pulse waveform, the use of controlled pulse waveform has a positive effect on molten zone to remove the porosity and minimize the bump. However, the rapid cooling after welding process would generate the coarse carbon particles and lack of fusion defect in the molten zone. Therefore, an improvement of heat input at the end of laser pulse is necessary by introducing an approach of ramp-down on the phase two to relieve the internal stress during re-solidification process, which would generate a better welded joint. The new controlled pulse waveforms are expressed as the annealing pulse waveform, and the trailing pulse waveform is also shown in Figure 18, in which the setting profile and the actual signal of three controlled pulse waveforms are also shown. Since the phase two of spike pulse waveform generated a stable weld bead compared with the rectangular pulse waveform, the amount of energy at the phase two for the annealing and the trailing pulse waveforms was conducted under the same energy of 420 mJ. The main difference between the annealing and the trailing pulse waveforms are the laser power and irradiation time during the phase two. The annealing pulse waveform has the higher laser power with the shorter

interaction time, while the trailing pulse waveform has the lower laser power with the longer interaction time.

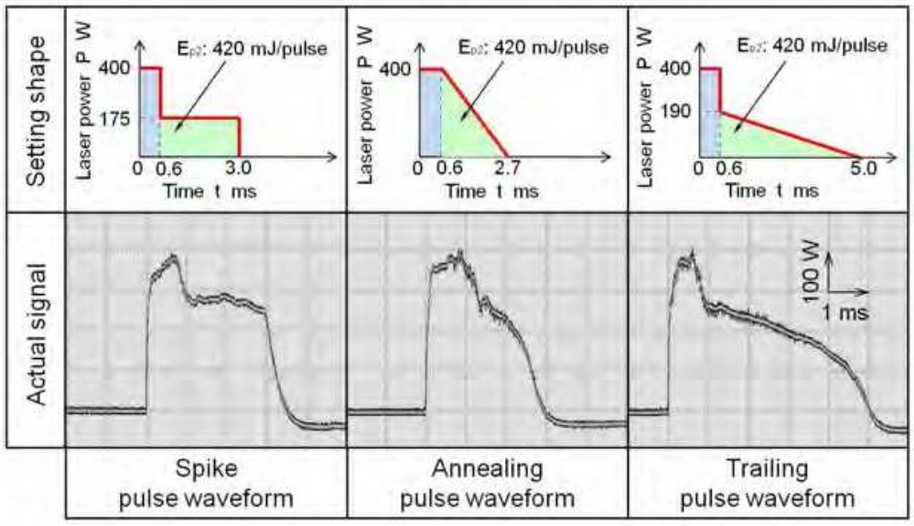

Fig. 18. Setting shape and actual signal of controlled pulse waveform

The difference of temperature change by spike, annealing and trailing pulse waveforms was investigated with the thermal calculation. Spike, annealing and trailing pulse waveforms are finished at the time of 3.0 ms, 2.7 ms and 5.0 ms, respectively. The temperature distributions were similar until 0.6 ms for three pulse waveforms, since they have similar pulse shape (laser power and pulse width) at the phase one. The main difference appeared at the pulse shape of phase two even under the same energy (E_{p2}: 420 mJ). Figure 19 and 20 show the temperature histories and distributions by these three controlled pulse waveforms. It can be seen that spike pulse waveform shows the constant temperature distribution during the phase two. Therefore, it is considered that the rapid cooling at 3 ms during the solidification generates internal stress, and it might cause the lack of fusion defect. From this disadvantage of spike pulse waveform, the slow cooling process is required during the solidification phase. As shown in the figures, the annealing pulse waveform shows the rapid decreasing of temperature distribution at the phase two. On the other hand, the trailing pulse waveform indicates the gradual decreasing of temperature distribution at the phase two, which means that slow cooling could be realized. In other words, the longer time of laser irradiation is useful at the phase two in order to overcome the lack of fusion problem.

SEM images and EDS mappings of cross-section with annealing and trailing pulse waveforms are shown in Figure 21. In the SEM image, the shape of molten zone can be seen clearly if there are existences of aluminum element on the Al-Gr composite material. Compared with the spike pulse waveform, the size of carbon particles was much smaller in the case of annealing pulse waveform. However, it shows that the lack of fusion was appeared around the carbon particles. In the case of trailing pulse waveform, it can be seen that the specimens have been molten well with an acceptable weld bead state without lack of fusion defect. It also shows that a better weld bead state was obtained by applying the trailing pulse waveform. Furthermore, the sufficient long time during welding process. In

other words, the slow cooling process during re-solidification is necessary to avoid the appearance of carbon particles and minimize the lack of fusion defect in the molten zone.

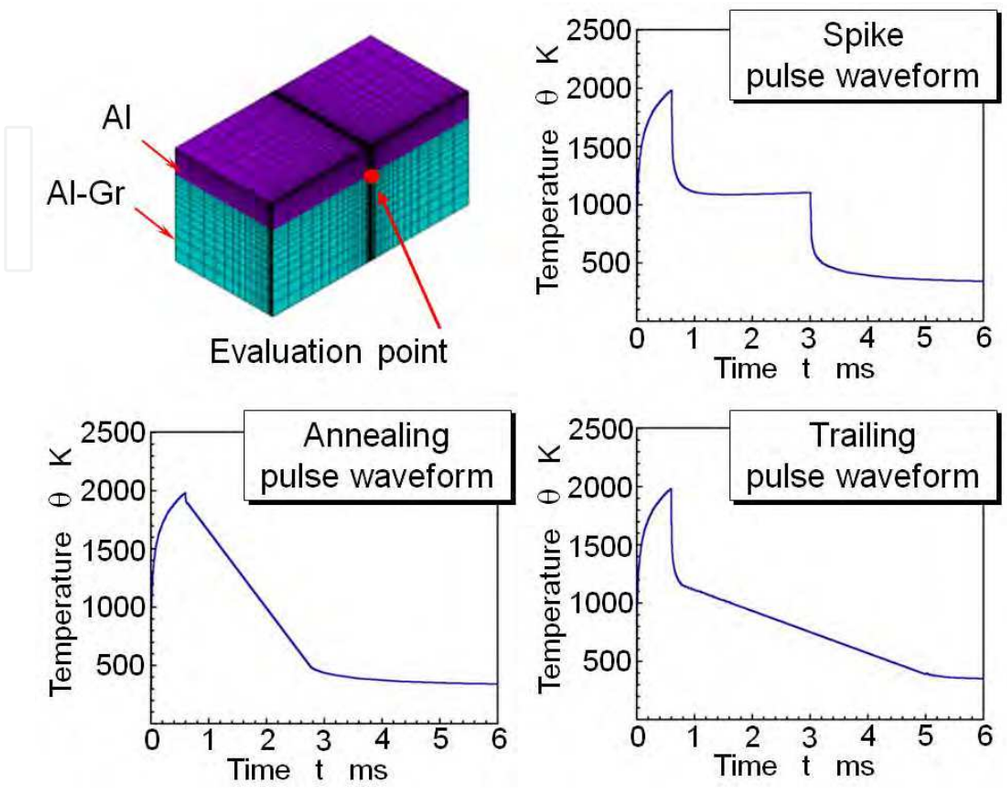

Fig. 19. Temperature histories by three controlled pulse waveforms

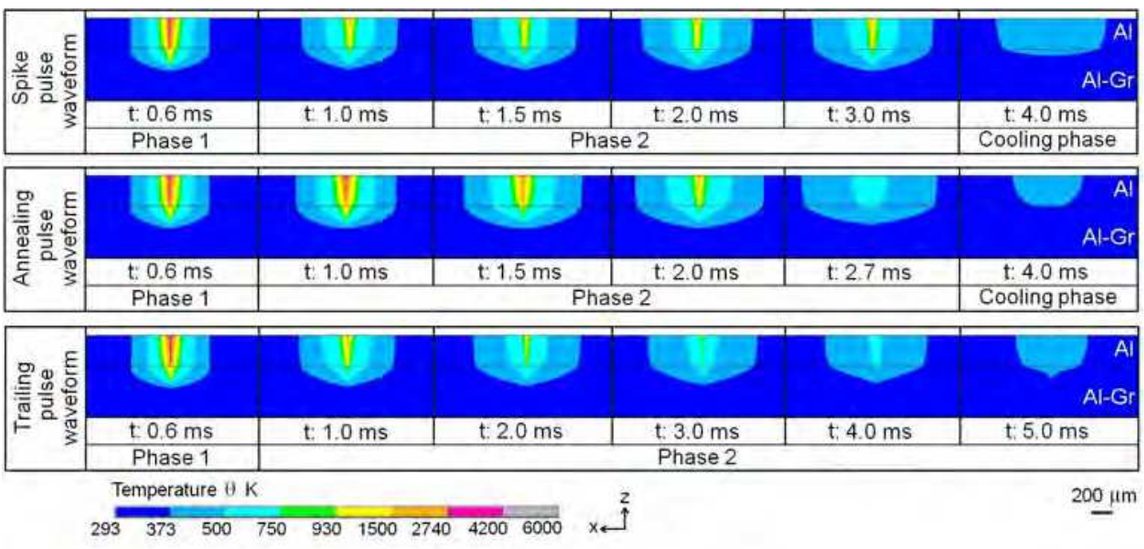

Fig. 20. Spatial temperature distribution by three controlled pulse waveforms

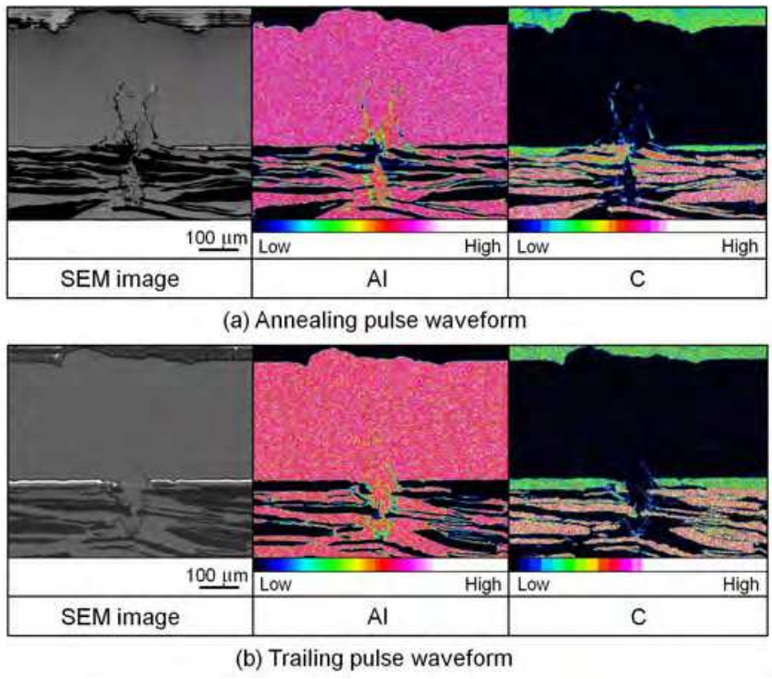

Fig. 21. SEM images and EDS mappings of cross-section with (a) annealing and (b) trailing pulse waveforms

6.3 Evaluation of mechanical strength

In order to evaluate the weld strength on the overlap welding with and without the control of pulse waveform under the constant laser pulse energy (E_P: 660 mJ/pulse), the shearing test was carried out. Figure 22 shows the shear strength for various laser pulse waveforms. As shown in the figure, the weld joint with controlled trailing pulse waveform indicated the greater weld strength compared to the uncontrolled pulse waveform. The lower strength of the uncontrolled pulse waveform is attributable to the fact that the existence of porosity reduced the strength of weld joint. Meanwhile, it shows that the spike pulse waveform was less significant to increase the weld strength compared to the uncontrolled pulse waveform. It can be noted that the lack of fusion defect was affected on the lower weld strength. Therefore, it is cleared that the the appropriate controlled laser pulse configurations are effective to improve the weld joint between aluminum and STC Al-Gr composite.

Figure 23 shows the fracture part on the top surface of Al-Gr composite after the shearing test. As can be seen from the figure, the fracture with uncontrolled pulse waveform occurred at the weld bead boundary in the Al-Gr composite and the presence of groove could be observed. It could be noticed that the existence of groove defect clearly influenced the weakness of weld joint strength. However, the fracture in the welding with the control of pulse waveform appeared inside the weld bead, which is located at the interface between pure aluminum and Al-Gr composite without the groove defect. In other words, the interfaces of aluminum and STC Al-Gr composite were expected to be the weak points of the weld joint. It is also considered that a weld joint without weld defects would increase the weld strength.

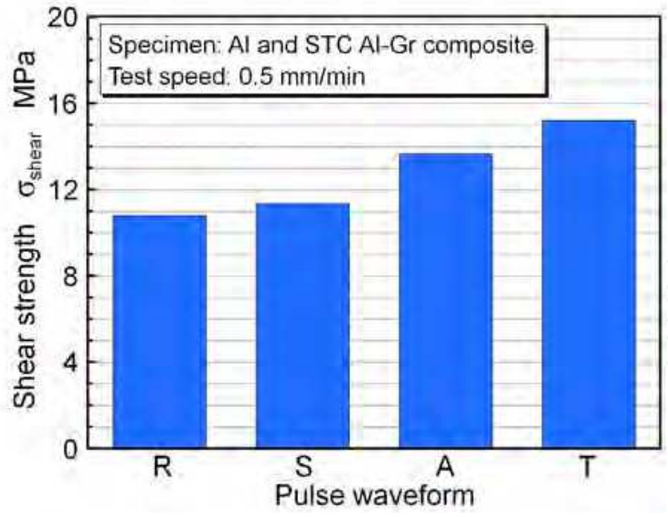

Fig. 22. Shear strength of the welding with and without the control of pulse waveforms (R: Rectangular, S: Spike, A: Annealing, T: Trailing)

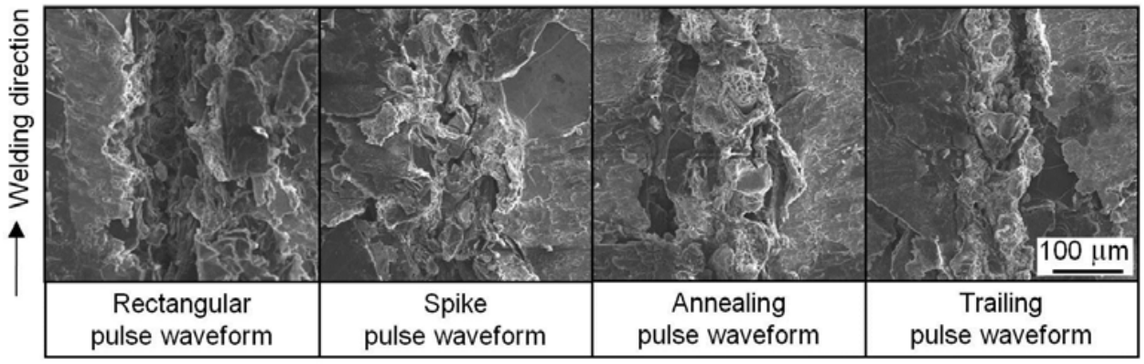

Fig. 23. SEM photographs of fracture on the top of STC Al-Gr composite

Figure 24 shows the side fracture surface of aluminum and STC Al-Gr composite, which were obtained from the shearing test under the welding condition with trailing pulse waveform. It can be seen that the fracture appearances show the brittle fracture. This fracture along the welding interface would deteriorate the weld strength of aluminum and STC Al-Gr composite joint. Figure 24 also shows the distribution map of elements Al and C on the fracture zone, where spot analysis of points 1 to 10 are listed in Table 3. It can not be detected the aluminum carbide Al_4C_3 at the fracture zone, since the solid graphite can not be solidified into liquid aluminum. EDS mapping on the bottom surface of aluminum confirms that after the shearing test, the fine and coarse graphite particles were found sticks on melted aluminum without mixture with solidified aluminum.

In the case of fracture zone on the top surface of STC Al-Gr composite, it also can be seen that the solidified aluminum was squeezed out towards the edge of weld joint region, which showed the aluminum and graphite can not mixed together between both materials.

Furthermore, the formation of the Al_4C_3 during welding process was successfully prevented during the welding process, which could deteriorate the strength of weld joint. In addition, the SEM observation revealed the crack was propagated in the fracture zone, which restricts the further strength of weld joint. However, compared to the bending strength of STC Al-Gr composite which is 7 MPa in the thickness direction, the weld strength between the aluminum and STC Al-Gr composite showed the relatively higher strength. Therefore, it is clearly performed that the controlled laser pulse configurations are effective to produce a higher strength of joint for welding between an aluminum and STC Al-Gr composite.

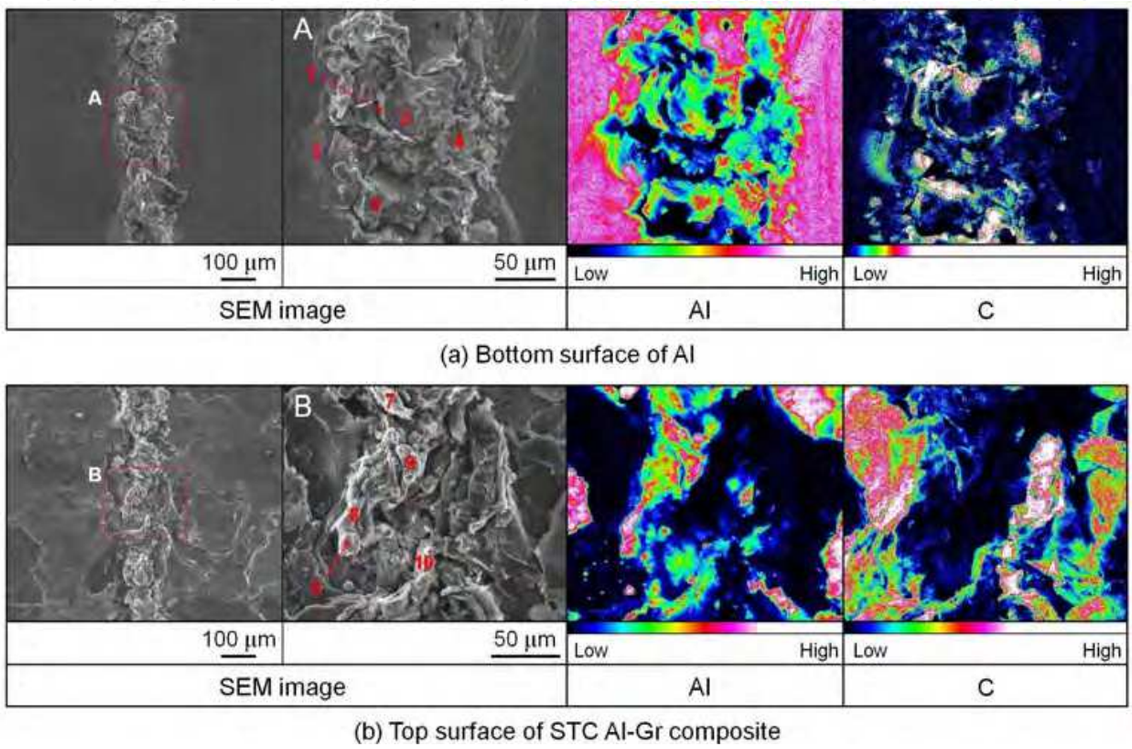

Fig. 24. SEM photographs and EDS mappings of fracture with trailing pulse waveform on the (a) bottom surface of aluminum and (b) top surface of STC Al-Gr composite

Point No.		1	2	3	4	5	6	7	8	9	10
Al	wt. %	49.67	30.94	62.84	41.16	64.45	52.45	35.68	48.66	64.65	48.01
C	wt. %	50.33	69.06	37.16	58.84	35.55	47.55	64.32	51.34	35.35	51.99

Table 3. Element composition of points 1-10 in Figure 24

7. Conclusion

The pulsed Nd:YAG laser micro-welding of a super thermal conductive (STC) aluminum-graphite composite was experimentally and numerically investigated. In the bead-on-plate welding of STC Al-Gr composite, the laser power and pulse width had a great influence on the top surface condition of weld bead. Laser power more than 30 W was required to melt

the STC Al-Gr composite without evaporation of the graphite element in the composite. The graphite was not mixed with aluminum during welding process to prevent the formation of aluminum carbide, which can degrade the weld joint. The overlap welding of aluminum and STC Al-Gr composite was successfully carried out using an appropriate controlled pulse waveform. Porosity and bump were observed as remarkable weld defects in overlap welding without a control of laser pulse. The proper control of laser power and pulse width could perform a positive result with largely free of weld defects and a relatively small bump. The controlled pulse waveform with slow cooling at the end of laser pulse was essential to relieve internal stress during solidification, since the lack of fusion was observed on the joining zone due to the rapid cooling. The higher shearing strength could be obtained by the control of pulse waveform compared with the uncontrolled rectangular pulse waveform.

8. Acknowledgment

The authors are grateful to Shimane Institute for Industrial Technology for supplying super thermal conductive aluminum-graphite composites.

9. References

Baraker, N.; Tzamtzis, S.; Dhindaw, B.K.; Patel, J.; Babu, N.H. and Fan, Z. (2009). Processing of Aluminum-Graphite Particulate Metal Matrix Composites by Advanced Shear Technology. *Journal of Materials Engineering and Performance,* Vol.18, No.9, pp. 1230-1240, ISSN 1059-9495

Bassani, P.; Capello, E.; Colombo, D.; Previtali, B. and Vedani, B. (2007). Effect of Process Parameters on Bead Properties of A359/SiC MMCs Welded by Laser. *Composites: Part A,* Vol.38, pp. 1089-1098, ISSN 1359-835X

Behler, K.; Berkmanns, J.; Ehrhardt, A. and Frohn, W. (1997). Laser Beam Welding of Low Weight Materials and Structures. *Materials and Design,* Vol.18, No.4/6, pp. 261-267, ISSN 0261-3069

Cao, X.; Wallace, W.; Poon, C. and Immarigeon, J.P. (2003). Research and Progress in Laser Welding of Wrought Aluminum Alloys – Laser Welding Processes. *Materials and Manufacturing Processes,* Vol.18, No.1, pp. 1-22, ISSN 1042-6914

Canilloo, V.; Sola, A.; Barletta, M. and Gisario, A. (2010). Surface Modification of Al-Al_2O_3 Composites by Laser Treatment. *Optics and Lasers in Engineering,* Vol.48, pp. 1266-1277, ISSN 0143-8166

Joseph, M.; Sivakumar, N. and Manoravi, P. (2002). High Temperature Vapour Pressure Studies on Graphite Using Laser Pulse Heating. *Carbon,* Vol.40, No.11, pp. 2031-2034, ISSN 0008-6223

Kannatey-Asibu, E. (2009). *Principles of Laser Materials Processing,* John Wiley & Sons, ISBN 978-0-470-17798-3, United State

Kirillin, A.V. and Kostanovskii, A.V. (2003). Melting Point of Graphite and Liquid Carbon. *Physics-Uspekhi,* Vol.46, No.12, pp. 1295-1303, ISSN 1063-7869

Kutz, M. (2002). *Handbook of Materials Selection,* John Wiley & Sons, Inc., ISBN 0-471-35924-6, Canada

Lienert, T.J.; Brandon, E.D. and Lippold, J.C. (1993). Laser and Electron Beam Welding of SiCp Reinforced Aluminum A-356 Metal Matrix Composite. *Scripta Metallurgica,* Vol.28, pp. 1341-1346, ISSN 0956-716X

Lu, H.; Shen, D.H.; Deng, X.F.; Xue, Q.K.; Froumin, N. and Polak, M. (2001). Study of the Al/Graphite Interface. *Chinese Physics,* Vol.10, No.9, pp. 832-835, ISSN 1009-1963

Massalski, T.B.; Okamoto, H.; Subramanian, P.R. and Kacprzak, L. (1990). *Binary Alloy Phase Diagrams (Vol.1),* ASM International, ISBN 0871704048, United State

Niu, J.; Pan, L.; Wang, M.; Fu, C. and Meng, X. (2006). Research on Laser Welding of Aluminum Matrix Composite SiCw/6061. *Vacuum,* Vol.80, pp. 1396-1399, ISSN 0042-207X

Pan, L.K.; Wang, C.C.; Hsiao, Y.C. and Ho, K.C. (2004). Optimization of Nd:YAG Laser Welding onto Magnesium Alloy via Taguchi Analysis. *Optics and Laser Technology,* Vol.37, pp. 33-42, ISSN 0030-3992

Ueno, T.; Yoshioka, T.; Ogawa, J.; Ozoe, N.; Sato, K. and Yoshino, K. (2009). Highly Thermal Conductive Metal/Carbon Composites by Pulsed Electric Sintering. *Synthetic Metals,* Vol.159, pp. 2170-2172, ISSN 0379-6779

Wang, H.M.; Chen, Y.L. and Yu, L.G. (2000). In-situ Weld-Alloying/Laser Beam Welding of SiCp/6061Al MMC. *Materials Science and Engineering,* Vol.A293, pp. 1-6, ISSN 0921-5093

Yue, T.M.; Xu, J.H. and Man, H.C. (1997). Pulsed Nd:YAG Laser Welding of SiC Particulate Reinforced Aluminium Alloy Composite. *Applied Composite Materials,* Vol.4, pp. 53-64, ISSN 0929-189X

Zhang, J.; Weckman, D.C. and Zhou, Y. (2008). Effect of Temporal Pulse Shaping on Cracking Susceptibility of 6061-T6 Aluminum Nd:YAG Laser Welds. *Welding Journal,* Vol.87, No.1, pp. 18s-30s, ISSN 0043-2296

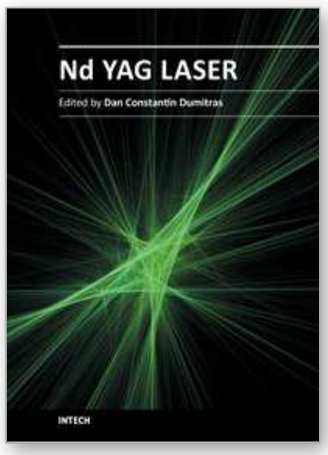

Nd YAG Laser

Edited by Dr. Dan C. Dumitras

ISBN 978-953-51-0105-5
Hard cover, 318 pages
Publisher InTech
Published online 09, March, 2012
Published in print edition March, 2012

Discovered almost fifty years ago at Bell Labs (1964), the Nd:YAG laser has undergone an enormous evolution in the years, being now widely used in both basic research and technological applications. Nd:YAG Laser covers a wide range of topics, from new systems (diode pumping, short pulse generation) and components (a new semiorganic nonlinear crystal) to applications in material processing (coating, welding, polishing, drilling, processing of metallic thin films), medicine (treatment, drug administration) and other various fields (semiconductor nanotechnology, plasma spectroscopy, laser induced breakdown spectroscopy).

How to reference

In order to correctly reference this scholarly work, feel free to copy and paste the following:

Mohd Idris Shah Ismail, Yasuhiro Okamoto and Akira Okada (2012). Micro-Welding of Super Thermal Conductive Composite by Pulsed Nd:YAG Laser, Nd YAG Laser, Dr. Dan C. Dumitras (Ed.), ISBN: 978-953-51-0105-5, InTech, Available from: http://www.intechopen.com/books/nd-yag-laser/micro-welding-of-super-thermal-conductive-composite-by-pulsed-nd-yag-laser

INTECH
open science | open minds

InTech Europe
University Campus STeP Ri
Slavka Krautzeka 83/A
51000 Rijeka, Croatia
Phone: +385 (51) 770 447
Fax: +385 (51) 686 166
www.intechopen.com

InTech China
Unit 405, Office Block, Hotel Equatorial Shanghai
No.65, Yan An Road (West), Shanghai, 200040, China
中国上海市延安西路65号上海国际贵都大饭店办公楼405单元
Phone: +86-21-62489820
Fax: +86-21-62489821

IntechOpen